*Journal of The Electrochemical Society*, **147** (3) 953-959 (2000)
S0013-4651(99)07-093-7 CCC: $7.00 © The Electrochemical Society, Inc.


# Two-Dimensional Simulation of Direct Methanol Fuel Cell

## A New (Embedded) Type of Current Collector

**A. A. Kulikovsky,[a,z] J. Divisek, and A. A. Kornyshev**

*Institute for Materials and Processes in Energy Systems, Jülich Research Center, D-52425 Jülich, Germany*

A two-dimensional numerical model of the direct methanol fuel cell with gas fuel is developed. Simulation of the cell with current collectors of conventional geometry reveal the formation of fuel-depleted, "shaded" regions in the cathode and anode catalyst layers. These regions are positioned in front of current collectors, farther from the gas channel windows. Another disadvantage of the conventional geometry is the concentration of electron current at the edges of current collectors. Based on the simulation results, a new design of current collectors is suggested. It is beneficial to position current collectors inside the backing and catalyst layers, parallel to the flow of the fuel. These embedded collectors do not produce shaded regions in the catalyst layers. Two plausible geometries of such collectors are considered: of rectangular and circular shape. Simulations show that depending on the transport properties of the backing and catalyst layers the embedded current collectors may significantly improve the performance of the fuel cell. This conclusion is valid also for hydrogen-oxygen fuel cells.
© 2000 The Electrochemical Society. S0013-4651(99)07-093-7. All rights reserved.

Manuscript submitted July 22, 1999; revised manuscript received November 15, 1999.

Direct methanol fuel cells (DMFC) are considered as promising sources of electrical power for vehicles. Although conventional hydrogen-oxygen fuel cells exhibit better performance, methanol has much higher energy density. Besides, methanol is much easier to produce, store, and transport than hydrogen.

Electrical current in DMFC is generated due to direct ionization of methanol at the anode

$$CH_3OH + H_2O \rightarrow CO_2 + 6H^+ + 6e^- \quad [1]$$

Protons then move to the cathode, where they recombine with the participation of oxygen

$$\frac{3}{2}O_2 + 6H^+ + 6e^- = 3H_2O \quad [2]$$

and hence the overall reaction is

$$CH_3OH + \frac{3}{2}O_2 \rightarrow CO_2 + 2H_2O \quad [3]$$

As the by-products are water and carbon dioxide, environmental pollution is minimal.

The structure of a conventional DMFC is shown in Fig. 1. Feed gases (methanol at the anode and oxygen at the cathode) are supplied through the gas channels in the highly conductive current collectors. These fuels then pass through the gas diffusion layers, DA and DC, and reach the anode and cathode catalyst layers, RA and RC, respectively, where reactions 1 and 2 take place. The anode and cathode compartments are separated by a proton-conducting membrane (currently made of polymer electrolyte), which should prevent the transport of the fuels.

Reactions 1 and 2 occur at the catalyst particles. Protons move in the polymer electrolyte, and electrons move along carbon threads, whereas methanol and oxygen are transported to reaction sites mainly via pores. The catalyst layers are the mixtures of the carbon particles covered by Pt or Pt-Ru catalyst in contact with the polymer electrolyte, with carbon threads and voids between them. The function of the carbon phase is to provide transport of electrons from/to the reaction sites, while the role of the void is to provide the delivery of the fuel/oxygen to the reaction sites.

During the past decade significant efforts have been directed toward the creation of low cost and effective DMFC. The state-of-the-art has recently been reviewed in Ref. 1. At the temperatures of liquid methanol, reaction kinetics are too slow; methanol is poorly consumed in the anode. The rest of it diffuses through the membrane to the cathode and reacts there with water and oxygen. This leads to a drastic reduction of the fuel-cell performance. Methanol vapor cells, that operate at elevated temperatures, are currently in the center of attention, as the methanol ionization runs faster there.

Numerical models of the DMFC have been developed in Ref. 2 and 3. In many aspects these models are similar to the models of conventional, hydrogen-oxygen polymer electrolyte fuel cell (PEFC).[4,5] All these models are one-dimensional; it is assumed that the cell is uniform in the lateral direction and the transport and kinetic processes vary only across the cell.

However, the gas channels only partially contact the gas diffusion layers (Fig. 1). There are, therefore, two sources of two-dimensional (2D) effects: nonuniform distributions of the gases concentrations and of electric potential in the carbon phase along *y* axis.

In Ref. 6 a 2D numerical model of the cathode compartment of a PEFC has been developed. In this work we extend this model to a description of the whole cell, both for the conventional geometry of current collectors and for a new geometry which comes out logically from our simulations.

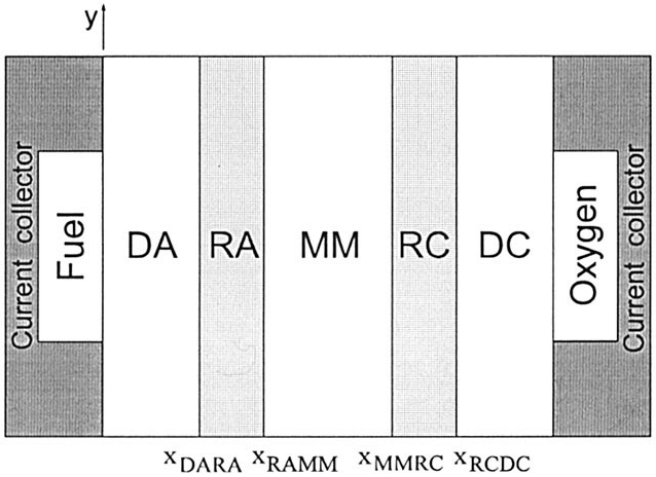


**Figure 1.** Sketch of the conventional cell. Abbreviations are: DA, anode diffusion layer; RA, anode reaction layer; MM, membrane; RC, cathode reaction layer; and DC, cathode diffusion layer. Notations of positions of the interfaces in the text.

[a] Permanent address: Research Computing Center, Moscow State University, 119899 Moscow, Russia.
[z] E-mail: akul@lem.srcc.msu.su

S0013-4651(99)07-093-7 CCC: $7.00 © The Electrochemical Society, Inc.

## The Model

In general, our model is based on mass conservation equations for concentrations of reacting species and conservation equations of proton and electron currents. Mass conservation in porous media leads to diffusion equations of a special type, which are described in a following section and in the Appendix. Following a commonly adopted approach, we introduce potentials of carbon and membrane phases, which are continuous functions of coordinates. The difference between them simulates the real distribution of the potential drop at the tortuous interface of carbon and polymer phases in the catalyst layers. Current conservation equations are coupled with the diffusion equations via source terms, which arise due to electrochemical reactions on both sides of the cell. The rate of electrochemical reactions depend exponentially on the potential difference, which make the problem nonlinear. In mathematical terms the model is two dimensional, as the properties of the system are invariant along one of the coordinates in the cell cross-sectional plane. This is a first step toward a full three-dimensional simulation. It represents, however, all the physical effects associated with the non-one-dimensional character of the current and gas flow distributions in the cell.

*Gas flow.*—We consider isothermal cell with gas fuel. It is assumed, that on both sides of the membrane there is no pressure gradient caused by external sources, *i.e.*, any pressure gradient due to different pressures on both sides of the cell is concentrated across the membrane. (Pressure gradient can be induced by the Knudsen diffusion in the catalyst layers. This gradient is taken into account in our model.)

The methanol crossover is an important issue in DMFC operation with liquid methanol feed. The crossover flux depends on membrane properties, current density, and pressure gradient across the membrane.[7] In a liquid-feed cell, the crossover flux can consume up to 30% of methanol. Besides, penetration of methanol through the membrane leads to a waste of oxygen in the cathode catalyst layer; both processes reduce cell efficiency.

The crossover flux in DMFC with gas methanol feed is much lower. Our experiments show that the methanol drag coefficient is then about four times lower. The crossover flux in a gas-fed DMFC does not exceed 10% of the total methanol flux, and to a first approximation it can be neglected. In this first attempt to construct a two-dimensional model of DMFC we consider an ideal membrane, impermeable for gases and fuel penetration. The extension of this model which takes into account methanol crossover will be published elsewhere.[8]

Transport of gases through the backing and catalyst layers is described within the scope of Rothfeld's model,[9] which takes into account both Stefan-Maxwell and Knudsen diffusion mechanisms

$$\frac{\mathbf{G}_k}{D_k^K} + \sum_l \frac{\xi_l \mathbf{G}_k - \xi_k \mathbf{G}_l}{D_{kl}} = -c\,\nabla\xi_k \qquad [4]$$

where $\xi_k$ and $G_k$ are relative molar concentration and flux of the $k$th component, respectively, $c$ the total molar concentration of a gas mixture, and $D_k^K$ and $D_{kl}$ are the Knudsen diffusion and Stefan-Maxwell binary diffusion coefficients, respectively.

The governing equation for each sort of molecule follows the mass balance

$$\nabla\cdot\mathbf{G}_k = R_k \qquad [5]$$

where $R_k$ is the rate of $k$th species production/consumption in electrochemical reactions. Taking divergence of Reaction 4 we get continuity equations for gases. This procedure and final form of mass balance equations are described in the Appendix.

*Potentials.*—The potentials of the membrane $\varphi_m$ and carbon phase at the anode $\varphi_a$ and cathode $\varphi_c$ obey the following equations

$$\nabla\cdot(\sigma_m\nabla\varphi_m) = \begin{cases} -R_a & x_{DARA} \le x \le x_{RAMM} \\ R_c & x_{MMRC} \le x \le x_{RCDC} \\ 0 & \text{otherwise} \end{cases} \qquad [6]$$

$$\nabla\cdot(\sigma_{ac}\nabla\varphi_a) = R_a \qquad [7]$$

$$\nabla\cdot(\sigma_{ac}\nabla\varphi_c) = -R_c \qquad [8]$$

where $\sigma_m$ and $\sigma_{ac}$ are the conductivities of the membrane and carbon phases, $R_a = R_a(\varphi_a - \varphi_m)$, and $R_c = R_c(\varphi_m - \varphi_c)$ (see Eq. 9, 10).

The symbols $x_{DARA}$, $x_{RAMM}$, $x_{MMRC}$, and $x_{RCDC}$ denote the positions of interfaces (Fig. 1).

*Rates of electrochemical reactions.*—The electrochemical reactions of methanol oxidation at the anode and oxygen reduction at the cathode are both complicated multistage processes. Thus the dependences of the corresponding reaction rates on the local value of $\varphi_{a,c} - \varphi_m$ may be determined by a system of equations each reflecting different stages, including adsorption and transformation of intermediates.[10-18] The result may have no relationship to a simple Butler-Volmer theory, although in different potential regions it may look like the Butler-Volmer form, or the Tafel one when far from equilibrium. In the latter case the result may be

$$R_a = i^0_{aref}\left(\frac{c_M}{c_{Mref}}\right)^{\gamma_a} \exp\left[\frac{\alpha_a F}{RT}(\varphi_a - \varphi_m)\right] \qquad [9]$$

$$R_c = i^0_{aref}\left(\frac{c_{O_2}}{c_{O_2 ref}}\right)^{\gamma_c} \exp\left[\frac{\alpha_c F}{RT}(\varphi_m - \varphi_c)\right] \qquad [10]$$

where the exponents in the dependence on the concentration of reactants may be quite different, and $\alpha$ coefficients, unlike in the Butler-Volmer theory, may exceed 1. As mentioned, these parameters at large potentials may be different from those in the range of moderate potentials. At least the values of $\alpha$ will be catalyst dependent, but due to the effects on the reaction mechanism the values of $\gamma$ may also be affected.

We do not go into details of a microscopic modeling of these reactions here, but rather parameterize the reaction rates by standard empirical approximations. Since we plot our results for sufficiently large currents, we use the simple exponential approximations, given by Eq. 9, 10. There is a variety of publications that report experimental evaluation of the parameters $\alpha$, $\gamma$ (see, *e.g.*, Ref. 19-25). They are often different in different potential ranges. In our simulation we use the parameters listed in Table I.

*Numerical details.*—Finite-difference approximations of model equations were constructed by the method of control volume, as described in Ref. 6. The computational domain was covered by an orthogonal grid. Potentials and concentrations are given at the nodes of the grid, whereas fluxes are given at the half-distance between the nodes (at the surfaces of computational cells).

An approximation of gas fluxes through the cell surface was obtained using the Sharfetter-Gummel scheme.[26] Equations for potentials were converted to finite-difference form with the usual five-point approximation. The detailed description of numerical aspects is given in Ref. 6.

A specific difficulty of the whole cell simulation is the problem for the membrane phase potential, where only derivatives of potential and the condition of periodicity are specified as the boundary conditions (Fig. 2). The position of potential surface $\varphi_m(x, y)$ is regulated by the additional condition of equality of total currents, generated at the anode and lost at the cathode. This condition stems from the following relations.

Integrating 6 over the volume between $x_{DARA}$ and $x_{RCDC}$ (Fig. 1), we get

$$\int_{V_{RA+MM+RC}} \nabla\cdot(\sigma_m\nabla\varphi_m)dV = -\int_{V_{RA}} R_a dV + \int_{V_{RC}} R_c dV \qquad [11]$$

where $V_{RA+MM+RC}$ stands for volume occupied by the anode catalyst layer (RA), membrane (MM), and cathode catalyst layer (RC),

S0013-4651(99)07-093-7 CCC: $7.00 © The Electrochemical Society, Inc.

**Table I. Conditions and parameters.**

| | Anode side | Cathode side |
|---|---|---|
| Cell temperature (°C) | 110 | |
| Gas pressure (atm) | 1.5 | 2.0 |
| Oxygen concentration in the gas channel | | 0.5 |
| Water concentration in the gas channel | 0.79 | 0.5 |
| Nitrogen concentration in the gas channel | | 0.0 |
| Methanol concentration in the gas channel | 0.20 | |
| $CO_2$ concentration in the gas channel | 0.01 | |
| $c_{O2,ref}$ (mol/cm$^3$) | | $3.18 \times 10^{-5}$ |
| $p_{M,ref}$ (atm) | 0.97 | |
| $i^0_{ref}$ (A/cm$^3$) | 1.0 | $1.0 \times 10^{-5}$ |
| α in Ref. 9, 10 | 0.5 | 2.0 |
| γ in Ref. 9, 10 | 1.0 | 0.5 |
| Mean pore radius in backing layer <*r*> (cm) | $10^{-5}$ | |
| Mean pore radius in catalyst layer <*r*> (cm) | $10^{-6}$ | |
| ϵ in Ref. 14 | 0.12 | |
| ψ in Ref. 15 | 0.156 | |
| Proton diffusion coeff. $D_H$ (cm$^2$/s) | $4.5 \times 10^{-5}$ | |
| Proton concentration $c_H$ (mol/cm$^3$) | $1.2 \times 10^{-3}$ | |
| Carbon-phase conductivity $\sigma_{ac}$ ($\Omega^{-1}$ cm$^{-1}$) | 40 | |
| Membrane phase conductivity $\sigma_m$ ($\Omega^{-1}$ cm$^{-1}$) | 0.034 | |
| Correction factor $\epsilon_M$ in Ref. 16 | 0.2 | |
| Catalyst layer thickness (cm) | 0.001 | |
| Backing layer thickness (cm) | 0.01 | |
| Membrane thickness | 0.02 | |

$V_{RA}$ and $V_{RC}$ are volumes of anode and cathode catalyst layers, respectively.

The integral on the left side of Eq. 11 can be transformed to the surface integral

$$\int_{V_{RA+MM+RC}} \nabla\cdot(\sigma_m \nabla\varphi_m) dV = \int_{S_{RA+MM+RC}} \sigma_m \nabla\varphi_m dS = 0$$

which is zero since the total ionic current passed through the surface $S_{RA+MM+RC}$ of the volume $V_{RA+MM+RC}$ is zero. Equation 11, therefore, reduces to

$$-\int_{V_{RA}} R_a dV + \int_{V_{RC}} R_c dV = 0 \qquad [12]$$

To satisfy relation 12, the following procedure was used. On each iteration the membrane-phase potential was updated according to the relation

$$\varphi_m \leftarrow \varphi_m + \frac{-\int_{V_{RA}} R_a dV + \int_{V_{RC}} R_c dV}{-\int_{V_{RA}} \frac{\partial R_a}{\partial \varphi_m} dV + \int_{V_{RC}} \frac{\partial R_c}{\partial \varphi_m} dV} \qquad [13]$$

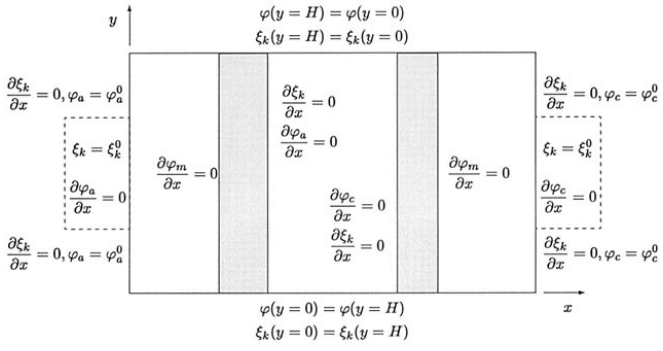


**Figure 2.** Boundary conditions for the cell with conventional current collectors.

which provides the fulfillment of Eq. 12 and thus gives correct solution to Eq. 6.

## Results and Discussion

*Parameters.*—All results presented below have been obtained for the parameters and conditions listed in Table I. Binary diffusion coefficients were calculated using the approximation (Ref. 27, p. 505) with the following correction for porosity ϵ

$$D_{kl} \rightarrow \epsilon^{1.5} D_{kl} \qquad [14]$$

These coefficients are listed in Table II.

The Knudsen diffusion coefficient is proportional to the product of mean pore radius and mean thermal velocity of the molecules

$$D_k^K = \psi <r> \sqrt{\frac{8RT}{\pi M_k}} \qquad [15]$$

where $T$ is the absolute temperature, $M_k$ the molecular weight of $k$th component, <*r*> the mean pore radius, and ψ a correction factor. Table III shows the values of Knudsen diffusion coefficients used in simulations. Due to the ten times lower mean pore radius in the catalyst layers, the Knudsen diffusion coefficients there are ten times less than in the backing layers.

The conductivity of the membrane phase was calculated according to the corrected Einstein relationship

$$\sigma_m = \epsilon_M \frac{F^2}{RT} D_H c_H \qquad [16]$$

where $D_H$ is the proton diffusion coefficient, $c_H$ the proton concentration in the membrane, and $\epsilon_M$ is a correction factor. With the parameters listed in Table I, this gives $\sigma_m \approx 0.034\ \Omega^{-1}\ cm^{-1}$. It is known that the proton conductivity of the bulk membrane exceeds the conductivity of the membrane phase in the catalyst layer. However, our aim is investigation of transport properties of the different electrode systems, and to simplify things we performed simulations with constant $\sigma_m$.

*Conventional geometry of current collectors.—Boundary conditions.*—The cell with the conventional geometry of current collectors is shown in Fig. 1. Gas channels are in contact with left/right side surface of the corresponding backing layer; the rest of this surface is in contact with current collector. For that case boundary conditions for gas molar concentrations and voltages are shown in Fig. 2. The anode gas problem is formulated in the domain $0 \le x_{RAMM}$ (Fig. 1). At the plane $x = 0$ there are two conditions on the gas concentration, zero flux (below and above the gas channel) and fixed concentration in the channel. At the interface with bulk membrane ($x = x_{RAMM}$), the fluxes of gases are assumed to be zero. The same conditions are imposed for gases at the cathode side.

**Table II. Binary diffusion coefficients (cm$^2$ s$^{-1}$).**

| $D_{MeCO2}$ | $D_{Mew}$ | $D_{CO2w}$ | $D_{N2O2}$ | $D_{N2w}$ | $D_{O2w}$ |
|---|---|---|---|---|---|
| 0.01740 | 0.02357 | 0.03198 | 0.02669 | 0.03867 | 0.03698 |

**Table III. Knudsen diffusion coefficients (cm$^2$ s$^{-1}$).**

| | $D^K_{Me}$ | $D^K_{CO2}$ | $D^K_{N2}$ | $D^K_{O2}$ | $D^K_w$ |
|---|---|---|---|---|---|
| BL | 0.0785 | 0.0670 | 0.08395 | 0.07853 | 0.10470 |
| CL | 0.00785 | 0.00670 | 0.00840 | 0.00785 | 0.01047 |

BL = backing layers; CL = catalyst layers.

S0013-4651(99)07-093-7 CCC: $7.00 © The Electrochemical Society, Inc.

On the bottom and top ends ($y = 0$, H) periodic boundary conditions for all variables are imposed. This means that the computational domain covers a part of the cell assembly which is repeated periodically along the $y$ axis.

The potential of the carbon phase at the anode side satisfies the following boundary conditions (Fig. 2). At $x = 0$ below and above the fuel channel, current collectors fix the potential: $\varphi_a = \varphi_a^0$. In the channel, the normal component of electron current density is zero, $\partial\varphi_a/\partial x = 0$. No electron current flows through the membrane interface, at $x = x_{RAMM}$. Similar boundary conditions are imposed for cathode potential.

The membrane phase potential is defined in the domain $x_{DARA} \leq x \leq x_{RCDC}$ (Fig. 1). On both the right and left sides of this domain the protons current normal to the surface of the corresponding catalyst layer is zero, that is, $\partial\varphi_m/\partial x = 0$ (Fig. 2). On the top and bottom surfaces, periodic boundary conditions are imposed.

*Currents and reaction rates.*—Figure 3 displays the distribution of current densities and reaction rates (mean current density in the cell is 0.2 A/cm$^2$). On both sides gases are supplied along the section $0.05 \leq y \leq 0.15$ cm; below and above this section, current collectors reside. The contour lines of electron current density in both the anode and cathode reveal strong peaks near the edges of current collectors (at $y = 0.05$ and $y = 0.15$ cm). These edges collect all the current which is produced opposite the gas channels. The peak current density is about ten times higher than the mean current density through the cell, and it may produce local Joule overheating.

The reaction rates $R_a$ and $R_c$ are reduced by the lack of methanol/oxygen in the top and bottom parts of the catalyst layers, shielded by current collectors, since the concentration of feed gases here is lower than on front of the gas channels.

*Plane embedded current collectors.*—To prevent partial shield of catalyst layers by current collectors, it is beneficial to insert current collectors into the sandwich of backing and catalyst layers *i.e.*, to position the surfaces of current collectors parallel to the fuel flow, as shown in Fig. 4 (embedded collectors). Boundary conditions for this problem are shown in Fig. 5.

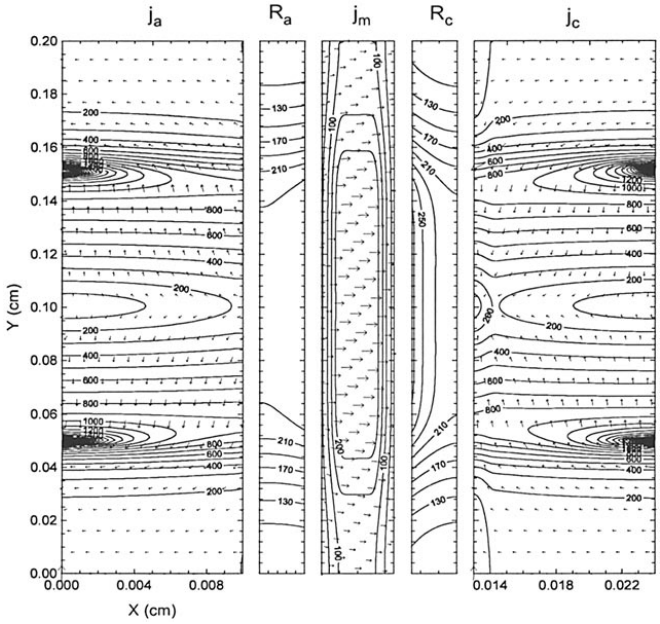


**Figure 3.** Cell with the conventional electrodes. Contour lines of electron current density at the anode $j_a$, at the cathode $j_c$, and in the membrane phase $j_m$ (mA/cm$^2$). Arrows indicate direction of electron and proton flow. $R_a$ and $R_c$ (A/cm$^3$) are contour lines of reaction rates in the anode and the cathode catalyst layers, respectively. The maps $R_a$ and $R_c$ are stretched along the $x$ axis to represent the details. Mean current density in the cell is 0.2 A/cm$^2$.

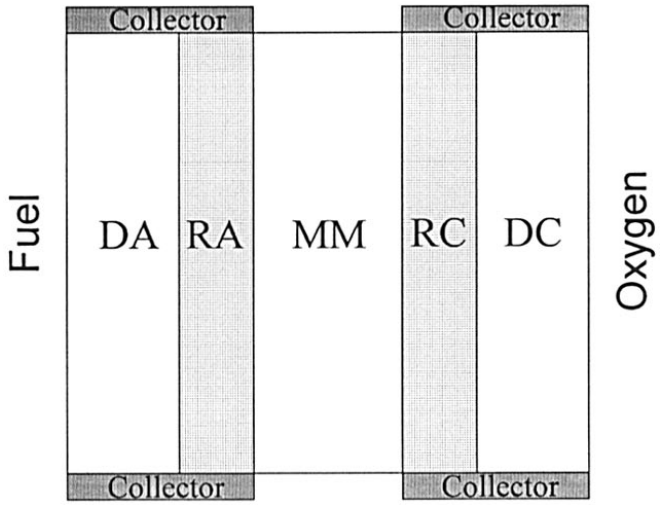


**Figure 4.** Sketch of the cell with the plane embedded current collectors. Abbreviations are the same as in Fig. 1.

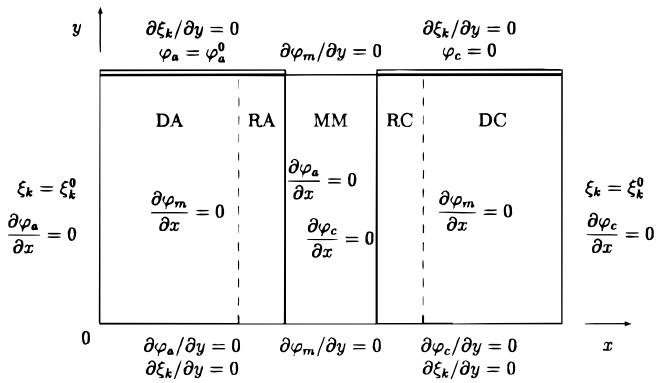


**Figure 5.** Boundary conditions for plane embedded current collectors (shown above by the double line). The problem has axis of symmetry ($y = 0$), where symmetry conditions for all variables are imposed.

Contour lines of current densities and reaction rates are shown in Fig. 6 (the mean current density through the cell again is 0.2 A/cm$^2$). It is seen, that the distribution of current densities along the surface of current collectors on the both sides is almost uniform. Reaction

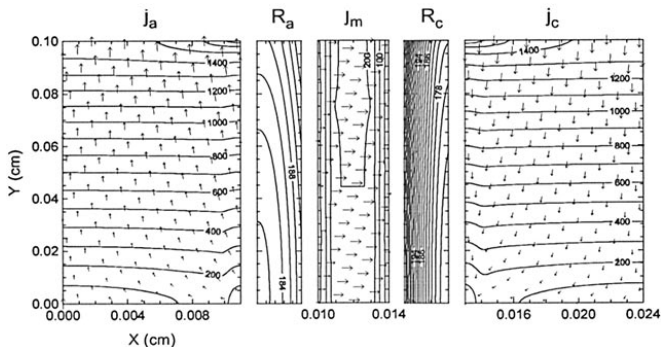


**Figure 6.** Cell with the plane embedded current collectors, positioned horizontally along $y = -0.1$ cm (not shown) and $y = 0.1$ cm. Contour lines of electron current density at the anode $j_a$, at the cathode $j_c$, and in the membrane phase $j_m$ (mA/cm$^2$). Arrows indicate direction of electron and proton flow. $R_a$ and $R_c$ (A/cm$^3$) are contour lines of reaction rates in the anode and the cathode catalyst layers, respectively. The maps $R_a$ and $R_c$ are stretched along the $x$ axis to represent the details. The mean current density in the cell is 0.2 A/cm$^2$.

S0013-4651(99)07-093-7 CCC: $7.00 © The Electrochemical Society, Inc.

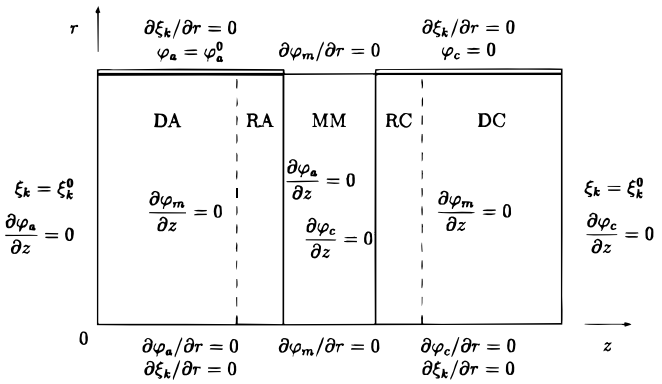


**Figure 7.** Boundary conditions for circular embedded current collectors (shown above by double line). The problem has axis of symmetry ($r = 0$), where symmetry conditions for all variables are imposed.

rates are also distributed almost uniformly along catalyst layers, due to uniform, along the *y* axis, flow of feed gases. The advantage of this geometry is evident. Note, that the flow of electrons in this case is perpendicular to the flow of protons.

*Circular embedded current collectors.*—The idea of embedded current collectors can be realized in a cylindrical geometry. In this case current collectors have a form of circular rings which bound the circular "sandwich" of a cell. The cell cross section looks like that shown in Fig. 4, being now a cross section of a cylindrical figure with the *z* axis directed horizontally. In order to simulate a cell of that geometry, model equations were rewritten in cylindrical coordinates. Boundary conditions for this problem are shown in Fig. 7.

Figure 8 shows the results. The distributions of current densities and reaction rates are similar to the case of plane-embedded collectors. We conclude that the actual form of embedded current collectors can be chosen in accordance with engineering requirements, which lie beyond the scope of this paper.

## Discussion

Figure 9 shows the distribution of methanol concentration in the anode with conventional current collectors and with the embedded ones. The shaded region in the catalyst layer of the anode with conventional collectors is clearly seen, whereas the new cell provides much more uniform (along the *y* axis) and higher concentrations of methanol in the catalyst layer.

Figure 10 shows voltage-current curves for the three considered types of current collectors. It is seen, that cells with embedded electrodes give better performance, regardless of their particular geometry. Moreover, our simulations show that these cells operate normally up to the current densities of the order 2 A/cm$^2$, whereas conventional cell has limiting current density of the order of 0.6 A/cm$^2$. This limiting current density is defined by poor fuel transport to the shaded regions of catalyst layer, opposite to the current collectors.

In the analysis presented above, it is implicitly assumed that in the case of embedded collectors the potential drop in the metal electrode is negligibly small. The validity of this assumption depends on the particular geometry and properties of embedded collectors as well as on the geometry of a stack element. The embedded collectors should be as thin as possible to increase the apparent power density of the stack element. This might be a subject of further experimental and engineering investigations.

Conventional current collectors considered in these simulations cover 50% of the backing layer surface. Sometimes "point" collectors are used, which cover only a small part of the backing-layer surface. This provides more uniform flow field of gases. However, such

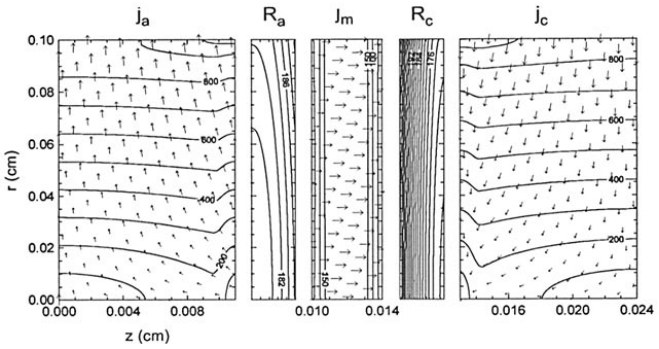


**Figure 8.** Cell of circular shape with the circular embedded current collectors, positioned along $r = 0.1$ cm. Contour lines of electron current density at the anode $j_a$, at the cathode $j_c$, and in the membrane phase $j_m$ (mA/cm$^2$). Arrows indicate direction of electron and proton flow. $R_a$ and $R_c$ (A/cm$^3$) are contour lines of reaction rates in the anode and the cathode catalyst layers, respectively. The maps $R_a$ and $R_c$ are stretched along the *x* axis to represent the details. Mean current density in the cell is 0.2 A/cm$^2$.

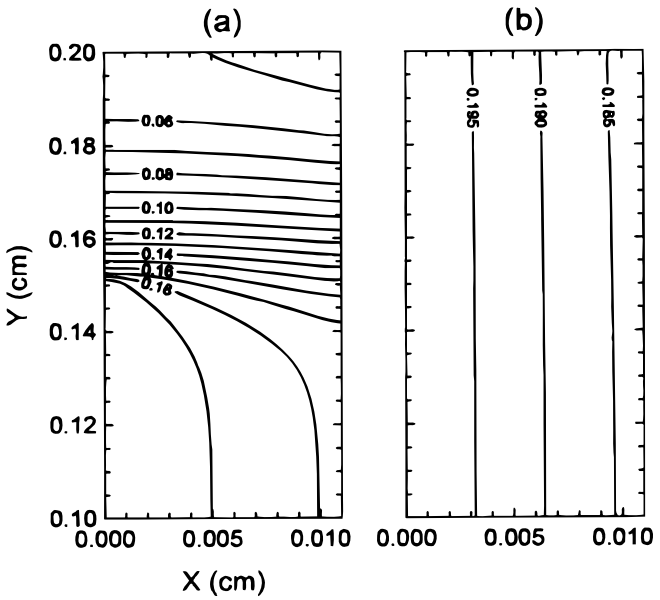


**Figure 9.** Methanol concentration in the cell with conventional current collectors (a) and with embedded ones (b). The map (a) is plotted for the upper half of the computational domain (see Fig. 3) for correct comparison with map (b).

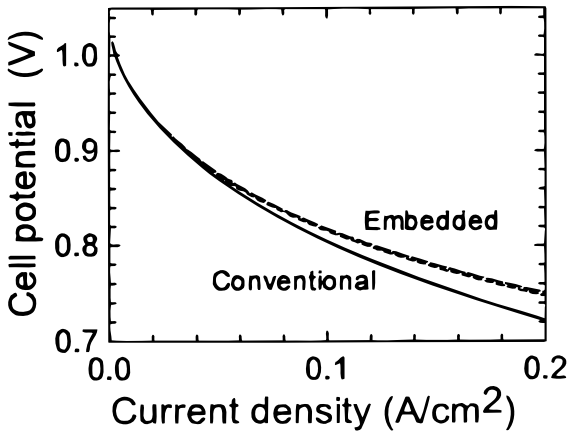


**Figure 10.** Voltage-current curves for the three cells considered. Lower (solid) curve is for the cell with the conventional geometry of current collectors. Both cells with embedded current collectors (plane and circular) give almost the same (dashed) curves with slightly better performance of the circular geometry.

S0013-4651(99)07-093-7 CCC: $7.00 © The Electrochemical Society, Inc.

collectors produce a strongly nonuniform distribution of electric potential in the carbon phase. As a result, the electron current is concentrated on the edges of the point-like collectors. Figure 3 shows, that this effect is rather strong even for conventional collectors, and it would be even stronger if one diminished the contact area with the carbon cloth. The embedded collectors are practically free from this drawback. The results presented show, that these collectors provide uniform distribution of gases along *y* axis and almost uniform distribution of carbon phase potential along the *x* axis. The simulation shows that the current density at the edge of conventional collector is about 6000 A/cm$^2$, whereas at the surface of the embedded collector it does not exceed 2000 A/cm$^2$.

## Conclusions

A two-dimensional model of the direct methanol fuel cell with gas feed is developed. (Similar investigation of DMFC with a liquid methanol feed is reported in Ref. 8.) The model is based on continuity equations for molar concentrations of gases and current continuity equations which govern the distributions of electrical potentials of membrane and carbon phases. Model equations are coupled by Butler-Volmer source terms which describe rates of electrochemical reactions in the anode and cathode catalyst layers.

It is shown that the conventional geometry of current collectors with gas channels leads to complex two-dimensional distributions of feed gas concentrations as well as of the potential of carbon phase. A shaded region forms behind the contact of the current collector plates and the diffuse layer, where there is a lack of methanol/oxygen. Another disadvantage of this geometry is the concentration of electron current at the edges of current collector/duffuse layer contacts, which may lead to local overheating of the electrode.

Based on the simulation results, a new geometry of current collectors (embedded collectors) is offered. The collectors can be embedded into the diffusion and catalyst layers so that no shaded regions in the "sandwich" arise. It is shown that the current density distribution along the surface of embedded collectors is almost uniform. The cell of the proposed new geometry gives better performance, has no two-dimensional diffusion limitations of gas transport to the reaction sites, and hence has a significantly higher limiting current density. Inhomogeneous Joule overheating in the new geometry should be minimal, and this would reduce degradation of membrane/electrode assembly.

## Acknowledgments

The authors are grateful to Dr. B. Steffen for a suggestion to use relation 13 in the numerical solution of the equation for the membrane phase potential.

*Research Center "Juelich" assisted in meeting the publication costs of this article.*

## Appendix

### *Equations of Mass Balance*

*Anode side.*—Relation 4 for the mixture of methanol, carbon dioxide, and water vapor have the following forms

$$\frac{\mathbf{G}_M}{D_M^K} + \frac{\xi_{CO2}\mathbf{G}_M - \xi_M\mathbf{G}_{CO2}}{D_{MCO2}} + \frac{\xi_w\mathbf{G}_M - \xi_M\mathbf{G}_w}{D_{Mw}} = -c\nabla\xi_M \quad [A\text{-}1]$$

$$\frac{\mathbf{G}_{CO2}}{D_{CO2}^K} + \frac{\xi_M\mathbf{G}_{CO2} - \xi_{CO2}\mathbf{G}_M}{D_{MCO2}} + \frac{\xi_w\mathbf{G}_{CO2} - \xi_{CO2}\mathbf{G}_w}{D_{CO2w}} = -c\nabla\xi_{CO2} \quad [A\text{-}2]$$

$$\frac{\mathbf{G}_w}{D_w^K} + \frac{\xi_M\mathbf{G}_w - \xi_w\mathbf{G}_M}{D_{Mw}} + \frac{\xi_{CO2}\mathbf{G}_w - \xi_w\mathbf{G}_{CO2}}{D_{CO2w}} = -c\nabla\xi_w \quad [A\text{-}3]$$

where the subscripts M, CO2, and w stand for methanol, carbon dioxide, and water, respectively. (For small methanol concentrations terms proportional to the methanol concentration $\xi_M$ in the left side of A-1 can be neglected. Relation A-1 then reduces to Fick's law for the methanol flux.)

Continuity equations for molar concentrations of gases are

$$\nabla\cdot\mathbf{G}_M = -\frac{S_M}{nF}R_a \quad [A\text{-}4]$$

$$\nabla\cdot\mathbf{G}_{CO2} = \frac{S_{CO2}}{nF}R_a \quad [A\text{-}5]$$

$$\nabla\cdot\mathbf{G}_w = -\frac{S_w}{nF}R_a \quad [A\text{-}6]$$

where $S$ is the stoichiometric coefficient, $n$ the number of electrons participating in the reaction, and $R_a$ the rate of charged-particle generation in the anode reaction.

Taking divergence of A-1, A-2, A-3, and taking into account A-4 to A-6 we get

$$\nabla\cdot\left(-c\nabla\xi_M + \left[\frac{\mathbf{G}_{CO2}}{D_{MCO2}} + \frac{\mathbf{G}_w}{D_{Mw}}\right]\xi_M\right) = \mathbf{G}_M\cdot\nabla\left(\frac{1}{D_M^K} + \frac{\xi_{CO2}}{D_{MCO2}} + \frac{\xi_w}{D_{Mw}}\right) - \left(\frac{1}{D_M^K} + \frac{\xi_{CO2}}{D_{MCO2}} + \frac{\xi_w}{D_{Mw}}\right)\frac{S_M}{nF}R_a \quad [A\text{-}7]$$

$$\nabla\cdot\left(-c\nabla\xi_{CO2} + \left[\frac{\mathbf{G}_M}{D_{MCO2}} + \frac{\mathbf{G}_w}{D_{CO2w}}\right]\xi_{CO2}\right) = \mathbf{G}_{CO2}\cdot\nabla\left(\frac{1}{D_{CO2}^K} + \frac{\xi_M}{D_{MCO2}} + \frac{\xi_w}{D_{CO2w}}\right) + \left(\frac{1}{D_{CO2}^K} + \frac{\xi_M}{D_{MCO2}} + \frac{\xi_w}{D_{CO2w}}\right)\frac{S_{CO2}}{nF}R_a \quad [A\text{-}8]$$

$$\nabla\cdot\left(-c\nabla\xi_w + \left[\frac{\mathbf{G}_{CO2}}{D_{CO2w}} + \frac{\mathbf{G}_M}{D_{Mw}}\right]\xi_w\right) = \mathbf{G}_w\cdot\nabla\left(\frac{1}{D_w^K} + \frac{\xi_M}{D_{Mw}} + \frac{\xi_{CO2}}{D_{CO2w}}\right) - \left(\frac{1}{D_w^K} + \frac{\xi_M}{D_{Mw}} + \frac{\xi_{CO2}}{D_{CO2w}}\right)\frac{S_w}{nF}R_a \quad [A\text{-}9]$$

Under given $\xi_k$, the relations A-1 to A-3 form the system of linear equations with respect to fluxes $\mathbf{G}_k$. Solving these equations one obtains fluxes which are then used in solving A-7 to A-9 for the molar concentrations of gases.

*Cathode side.*—Relation 4 for humidified air have the following forms

$$\frac{\mathbf{G}_{N2}}{D_{N2}^K} + \frac{\xi_{O2}\mathbf{G}_{N2} - \xi_{N2}\mathbf{G}_{O2}}{D_{N2O2}} + \frac{\xi_w\mathbf{G}_{N2} - \xi_{N2}\mathbf{G}_w}{D_{N2w}} = -c\nabla\xi_{N2} \quad [A\text{-}10]$$

$$\frac{\mathbf{G}_{O2}}{D_{O2}^K} + \frac{\xi_{N2}\mathbf{G}_{O2} - \xi_{O2}\mathbf{G}_{N2}}{D_{N2O2}} + \frac{\xi_w\mathbf{G}_{O2} - \xi_{O2}\mathbf{G}_w}{D_{O2w}} = -c\nabla\xi_{O2} \quad [A\text{-}11]$$

$$\frac{\mathbf{G}_w}{D_w^K} + \frac{\xi_{N2}\mathbf{G}_w - \xi_w\mathbf{G}_{N2}}{D_{N2w}} + \frac{\xi_{O2}\mathbf{G}_w - \xi_w\mathbf{G}_{O2}}{D_{O2w}} = -c\nabla\xi_w \quad [A\text{-}12]$$

where subscripts N2, O2, and w stand for nitrogen, oxygen, and water, respectively.

Continuity equations for molar concentrations of gases are

$$\nabla\cdot\mathbf{G}_{N2} = 0 \quad [A\text{-}13]$$

$$\nabla\cdot\mathbf{G}_{O2} = -\frac{S_{O2}}{nF}R_c \quad [A\text{-}14]$$

$$\nabla\cdot\mathbf{G}_w = \frac{S_w}{nF}R_c \quad [A\text{-}15]$$

where $S$ is the stoichiometric coefficient, $n$ the number of electrons, and $R_c$ rate of charged particles lost in Reaction A-2.

Taking the divergence of A-10, A-11, A-12, and taking into account A-13 to A-15 we get

S0013-4651(99)07-093-7 CCC: $7.00 © The Electrochemical Society, Inc.

$$\nabla\cdot\left(-c\nabla\xi_{N2}+\left[\frac{\mathbf{G}_{O2}}{D_{N2O2}}+\frac{\mathbf{G}_{w}}{D_{N2w}}\right]\xi_{N2}\right)=\mathbf{G}_{N2}\cdot\nabla\left(\frac{1}{D^{K}_{N2}}+\frac{\xi_{O2}}{D_{N2O2}}+\frac{\xi_{w}}{D_{N2w}}\right) \quad [A\text{-}16]$$

$$\nabla\cdot\left(-c\nabla\xi_{O2}+\left[\frac{\mathbf{G}_{N2}}{D_{N2O2}}+\frac{\mathbf{G}_{w}}{D_{O2w}}\right]\xi_{O2}\right)=\mathbf{G}_{O2}\cdot\nabla\left(\frac{1}{D^{K}_{O2}}+\frac{\xi_{N2}}{D_{N2O2}}+\frac{\xi_{w}}{D_{O2w}}\right)-\left(\frac{1}{D^{K}_{O2}}+\frac{\xi_{N2}}{D_{N2O2}}+\frac{\xi_{w}}{D_{O2w}}\right)\frac{S_{O2}}{nF}R_{c} \quad [A\text{-}17]$$

$$\nabla\cdot\left(-c\nabla\xi_{w}+\left[\frac{\mathbf{G}_{O2}}{D_{O2w}}+\frac{\mathbf{G}_{N2}}{D_{N2w}}\right]\xi_{w}\right)=\mathbf{G}_{w}\cdot\nabla\left(\frac{1}{D^{K}_{w}}+\frac{\xi_{N2}}{D_{N2w}}+\frac{\xi_{O2}}{D_{O2w}}\right)+\left(\frac{1}{D^{K}_{w}}+\frac{\xi_{N2}}{D_{N2w}}+\frac{\xi_{O2}}{D_{O2w}}\right)\frac{S_{w}}{nF}R_{c} \quad [A\text{-}18]$$

Quite analogous to the situation at the anode, relations A-10 to A-12 form the system of linear equations with respect to fluxes $\mathbf{G}_k$. Solving this system one obtains fluxes which then are used to solve A-16 to A-18 for molar concentrations of gases.

## References


1. S. Gottesfeld and T. A. Zawodzinski, *Advances in Electrochemical Science and Engineering*, Vol. 5, R. C. Alkire, H. Gerischer, D. M. Kolb, and C. W. Tobias, pp. 195-301, Wiley, Weinheim (1998).
2. J. Wang and R. F. Savinell, in *Electrode Materials and Processes for Energy Conversion and Storage*, S. Srinivasan, D. D. Macdonald, and A. C. Khandkar, Editors, PV 94-23, p. 396, The Electrochemical Society Proceedings Series, Pennington, NJ (1994).
3. K. Scott, W. Taama, and J. Cruickshank, *J. Power Sources*, **65,** 159 (1997).
4. T. E. Springer, T. A. Zavodzinski, and S. Gottesfeld, *J. Electrochem. Soc.*, **138,** 2334 (1991).
5. D. M. Bernardi and M. W. Verbrugge, *J. Electrochem. Soc.*, **139,** 2477 (1992).
6. A. A. Kulikovsky, J. Divisek, and A. A. Kornyshev, *J. Electrochem. Soc.*, **146,** 3981 (1999).
7. X. Ren, T. A. Zawodzinski Jr., F.-Uribe, H.-Dai, and S.-Gottesfeld, in *Proton Conducting Membrane Fuel Cells 1*, S. Gottesfeld, G. Halpert, and A. Landgrebe, Editors, PV 95-23, p. 284, The Electrochemical Society Proceedings Series, Pennington, NJ (1995).
8. A. A. Kulikovsky, *J. Appl. Electrochem.* (1999), Submitted.
9. L. B. Rothfeld, *AIChE J.*, **9,** 19 (1963).
10. V. S. Bagotzky and Yu. B. Vasilyev, *Electrochim. Acta*, **9,** 869 (1964).
11. V. S. Bagotzky and Yu. B. Vasilyev, *Electrochim. Acta*, **11,** 1439 (1966).
12. V. S. Bagotzky and Yu. B. Vasilyev, *Electrochim. Acta*, **12,** 1323 (1967).
13. B. B. Damaskin, O. A. Petrii, and V. V. Batrakov, *Adsorption of Organic Compounds on Electrodes*, Plenum Press, New York (1971).
14. B. I. Podlovchenko and R. P. Petukhova, *Electrokhimiya*, **10,** 489 (1974).
15. M. R. Tarasevich, A. Sadkowski, and E. Yeager, in *Comprehensive Treatise of Electrochemistry*, Vol. 7, B. E. Convay, J. O'M. Bockris, E. Yeager, S. U. M. Khan, and R. E. White, Editors, pp. 310-398, Plenum Press, New York (1983).
16. B. E. Convay and E. D. Radd, in *Comprehensive Treatise of Electrochemistry*, Vol. 7, B. E. Convay, J. O'M. Bockris, E. Yeager, S. U. M. Khan, and R. E. White, Editors, pp. 641-771, Plenum Press, New York (1983).
17. J.-M. Leger and C. Lamy, *Ber. Bunsenges. Phys. Chem.*, **94,** 1021 (1990).
18. C. Lamy and J.-M. Leger, *J. Chem. Phys.*, **88,** 1649 (1991).
19. S. J. Ridge, R. I. White, Y. Tsou, R. N. Beaver, and G. A. Eisman, *J. Electrochem. Soc.*, **136,** 1902 (1989).
20. D. M. Bernardi and M. W. Verbrugge, *AIChE J.*, **37,** 1151 (1991).
21. A. S. Avico, V. Antonucci, V. Alderucci, E. Modica, and N. Giordano, *J. Appl. Electrochem.*, **23,** 1107 (1993).
22. A. Parthasarathy, C. R. Martin, and S. Srinivasan, *J. Electrochem. Soc.*, **138,** 916 (1991).
23. P. S. Kauranen, E. Skou, and J. Munk, *J. Electroanal. Chem.*, **404,** 1 (1996).
24. P. S. Kauranen and E. Skou, *J. Electroanal. Chem.*, **408,** 189 (1996).
25. T. J. Schmidt, H. A Gasteiger, and R. J. Behm, *Electrochem. Commun.*, **1,** 1 (1999).
26. D. L. Scharfetter and H. K. Gummel, *IEEE Trans. Electron. Devices*, **ED-16,** 64 (1969).
27. R. B. Bird, W. E. Stewart, and E. N. Lightfoot, *Transport Phenomena*, Wiley, New York (1960).